www.cadanda.com
Computer-Aided Design AND APPLICATIONS

Thin-walled Product Redesign with Reverse Engineering Modeling and Mechanical T-splines

Xiang Xue[1], Xiaolian Tang[2] and Xiaoyun Qiu[3]

[1]Nanjing Polytechnic Institute, njxuexiang@126.com
[2]Nanjing Polytechnic Institute, tangxiaolian@126.com
[3]Nanjing Polytechnic Institute, yunyun_qxy@163.com

Corresponding author: Xiang Xue, njxuexiang@126.com

Abstract. In modern, ever-changing markets, product redesign is an essential means to keep a company's competitive advantages in business. In this paper, we propose a new approach to streamline the redesigned workflow of thin-walled products by means of geometric reverse engineering (RE), isogeometric shell analysis, and T-spline surface (T-splines) modeling. Firstly, we apply RE technique to create a computer-aided design (CAD) model from one physical thin-walled product. Then, we convert this CAD model into mechanical T-splines (MT-splines), which are built on the T-splines and isogeometric shell analysis. MT-splines not only can achieve the direct mechanical analysis of redesigned products in computer-aided engineering (CAE) by skipping the costly meshing process but also possess the flexible shape editability that comes from the combination of geometric alteration and mechanical deformation, all of which considerably improve the efficiency of product redesign workflow. Additionally, we study and find a helpful connection between local-uniform refinement (LU-Refinement) of T-splines and isogeometric analysis (IGA) in this paper so that we can always ensure the analysis-suitability of locally-refined MT-splines, which is crucial to the mechanical deformation and analysis of MT-splines driven by IGA. Finally, two redesign examples of bike mudguard and car-door are provided to demonstrate the usefulness and effectiveness of our proposed redesign workflow, offering new thinking for integrating RE, CAD, and CAE in new product development.

Keywords: Product redesign, Geometric reverse engineering, T-splines refinement, Isogeometric analysis and design
DOI: https://doi.org/10.14733/cadaps.2025.958-975

1 INTRODUCTION

To better meet customer's needs in today's competitive market, industrial designers are asked to develop and introduce new products within a limited time continuously. Instead of creating a new

product design from scratch, designers normally choose to reuse one existing similar product as the basis for designing a new one [29]. By redesigning existing products, designers are capable of rapidly evolving their products to constantly improve the competitiveness of the company while considerably reducing the cost of product development. Because the visual appearance of the product is an important factor in enhancing customer experience, modifying the product shape has become one of the effective ways to achieve product redesign. In many cases, a product redesigned with a new pleasing appearance will be more competitive to attract customers than the old product whose shape is less attractive.

However, it is not always an easy task to redesign an existing product in practical application because many products that need to be improved in the modern industry frequently only have physical objects and lack their original CAD documents for some reason. Therefore, how to obtain a suitable CAD model as the basis for product redesign becomes a challenging task for designers. Fortunately, RE technique [5] makes it possible for designers to quickly recreate a 3D model in computer from physical object. This model reconstruction technique has been extensively used in many fields to improve the product development cycle, including the fields of aerospace, automobile, injection mold, medical equipment, and consumer products. In some major CAD systems like CATIA [6] and NX CAD [26], RE technique has been integrated as an important tool to facilitate product redesign. Some professional RE modeling tools are also developed with the aim of recreating a high-quality CAD model from 3D scanning data for product redesign, such as Geomagic Design X [14].

Once designers obtain the CAD model of physical product through RE modeling, they can readily build a new product design by making some shape alterations to this model. After that, redesigned CAD model needs to be imported into a CAE system to examine the feasibility in engineering, like checking its mechanical property. Hence, the data integration from CAD to CAE is also a crucial factor to affect the efficiency of product redesign workflow. CAD and CAE fields have a long-standing issue of data compatibility because they adopt different mathematical approaches to describe their respective models. One CAD model always needs to be converted into another CAE-suitable model before conducting the engineering analysis on a computer. Such a CAD-to-CAE conversion process is usually complicated and time-consuming, making it difficult to ensure a quick and efficient checking of engineering performance in CAE after each product redesign.

Therefore, RE modeling, shape modification, and CAE analysis are three important aspects of industrial product redesign. Some research has been done in these three directions and achieved some good results. For example, a parametric reverse modeling method is proposed in [34] to improve the redesign of the prismatic CAD model described by NURBS surfaces. This redesign method based on reverse modeling includes four key steps, which are strategy analysis, extraction of sectional curves, reconstruction of feature models, and parametric redesign. In [7], haptic modeling is integrated with reverse modeling to present a new redesign approach. The shape modification in product redesign can become more flexible and intuitive with the help of a haptic interface in the virtual world. In [36], a new product redesign method is proposed by integrating reverse modeling with deformation. In this method, the GSM tool in ThinkDesign [31] software is applied to facilitate the shape modification of the redesigned product. Besides, a reverse innovative design methodology is presented in [35] to streamline the development of new products. CAE analysis software packages, such as Abaqus [1], are integrated into this redesign method and are used to achieve the design verification so that the redesigned product can be continuously optimized based on analysis feedback. However, the CAE analysis in redesign workflow is still inefficient due to the incompatible issue between CAD and CAE models. Moreover, we have to use different tools to separately realize the shape modification and CAE analysis of redesigned product, like the GSM tool of ThinkDesign for geometric deformation and the Abaqus software package for CAE mechanical analysis. Besides, the rigid tensor-product scheme of NURBS surface limits its flexibility in shape modification when it comes to product redesign.

The IGA approach [18] proposed by Prof. Hughes in 2005 can significantly enhance the integration between CAD and CAE. It is because IGA uses the same set of spline basis functions to mathematically describe both CAD and CAE models so that CAE analysis can be directly performed

on the CAD model without relying on the complex and inefficient model conversion. These years, the IGA approach has been successfully applied in many CAE fields to improve the accuracy and efficiency of engineering analysis, such as in shell analysis and simulation [21][30], contact mechanics [23], structural vibration [9], aerodynamics [3], even the optics [2] and cardiac electrophysiology [4]. Some commercial CAE software, like LS-DYNA [17] and Abaqus [22], have also developed corresponding IGA modules on their platforms, hoping to make full use of the IGA approach in industry applications. Therefore, IGA is a promising engineering analysis approach and can be used to streamline the current product redesign workflow.

In the CAD industry, T-splines [28] are the superset of the popular Non-Uniform Rational B-Spline (NURBS) surface and accommodate flexible T-junctions on its surface structure. For the benefits of local refinability and exact compatibility to NURBS surface, T-splines are widely studied in CAD and CAE fields, like efficient local surface skinning [24] and adaptive isogeometric analysis [11]. Moreover, T-splines can also be applied to improve the efficiency of computer numerical control (CNC) manufacturing [13] and additive manufacturing (AM) [12]. For their advantages in CAD and CAE, T-splines will also be beneficial to product redesign in engineering, especially useful to the redesign of thin-walled products described by freeform surfaces.

Some research has been done in recent years to study the integration of RE/T-splines, T-splines/IGA, and IGA/RE. For example, T-splines are combined with RE in [19] to achieve the flexible geometric reconstruction of tree branch structures in blood vessels and arteries for medical applications. In [10], T-splines are used to increase the efficiency of IGA with much-reduced degrees of freedom in computational mechanics when handling the frictionless contact problem of large deformation. In [16], a RE framework based on IGA is proposed to improve the numerical modeling and simulation of deep-drawn thin shell components. Although these existing studies have made some progress in CAD and CAE fields, how to unify the RE, T-splines, and IGA to resolve engineering design problems has not been investigated to our knowledge, especially in the aspect of product redesign.

As seen in Figure 1, we will introduce a new approach in this paper to streamline the redesign workflow of thin-walled products that are extensively used in aircraft, automotive, ships, buildings, and consumer products based on the smooth integration of RE/T-splines/IGA. Firstly, the RE modeling tool is applied to create a suitable NURBS model from the scanned data of one physical thin-walled product. Then, MT-splines is built on this NURBS model through model conversion and isogeometric shell analysis. Based on the resulting MT-splines, we can achieve flexible shape manipulation and direct mechanical analysis, both of which will greatly enhance the efficiency of thin-walled product redesign from both aspects of CAD and CAE.

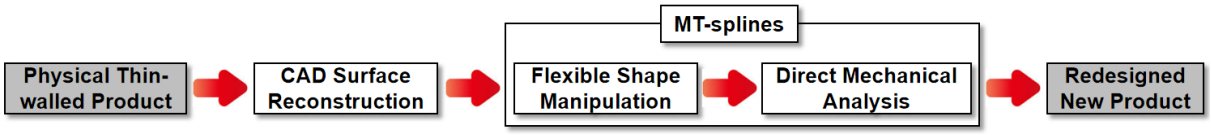

Figure 1: New redesign process for thin-walled products.

The rest of the paper is organized as follows. In Section 2, we briefly review the RE technique of geometric models. Section 3 offers a short description of T-splines and particularly investigates the LU-Refinement of T-splines. The construction of MT-splines based on isogeometric shell analysis is presented in Section 4, and Section 5 introduces the new redesign workflow for thin-walled products. Two redesign examples are given in Section 6 to show the effectiveness and usefulness of our proposed new approach. Finally, Section 7 concludes the paper and discusses our future research direction.

In this paper, we focus on the shape redesign of thin-walled product and restrict the discussion on the case of bicubic T-splines. Additionally, we will use different control polygons to distinguish the NURBS surface (black polygon), T-splines (green polygon) and MT-splines (red polygon).

2 REVERSE ENGINEERING MODELING

Broadly speaking, reverse engineering is a process that takes apart one existing object into some basic units and analyzes their internal relations to gain knowledge about how this object works. Many things in a wide range of fields can be reverse-engineered, like those in product design, military technology, software engineering, chemicals, and even the pharmaceutical industry. For the reconstruction of the geometric model in the product design field, the RE technique is used to build a CAD model from the physical product by utilizing contact or non-contact digital measuring devices when the original CAD data of this product is incomplete or unavailable.

A typical process of geometric RE for product redesign is shown in Figure 2 and can be divided into four steps. In the first step, a 3D scanning system is used to acquire the shape information about the physical product, obtaining a data set of point clouds to describe the product shape. In step 2, the resulting point-cloud data is processed sequentially through operations of registration, cleaning, simplification, and smoothing so as to produce a suitable mesh model for surface reconstruction. In step 3, surface fitting is applied to create an appropriate surface patch from each consistent region over the mesh model, generating a set of surface patches to represent the shape of the physical product. In the final step, these fitted surface patches are trimmed and smoothly stitched to build a basic CAD model for subsequent product redesign, completing the geometric reconstruction of the physical product.

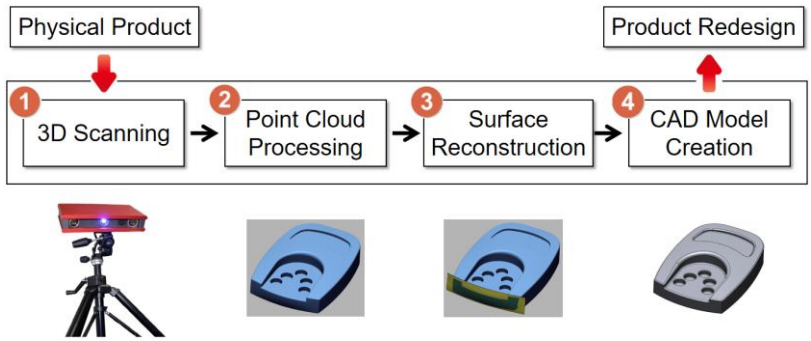

Figure 2: Geometric reverse engineering for product redesign.

With RE technique, designers are capable to quickly start a redesign work for those products that lack their original CAD documents, because it is no longer necessary for designers to laboriously redesign the product from scratch as in traditional product redesign cycle.

3 T-SPLINES AND LOCAL UNIFORM REFINEMENT

T-splines is an advanced geometry description for freeform surfaces in the CAD field. It has flexible local refinability and desirable exact compatibility with the popular NURBS surface. When refining the T-splines, we can add new control points in local rows or columns onto the surface rather than add full rows or columns of control points, which is unavoidable in NURBS refinements. Different from the NURBS surface based on tensor-product scheme, T-splines adopt the formulation of point-based splines (PB-splines) [28] by defining bicubic B-spline functions over a two-dimensional grid structure called T-mesh. Each bicubic B-spline function $B_i(u,v)$ determines its local support of

$(u_{i0},u_{i1},u_{i2},u_{i3},u_{i4})/(v_{i0},v_{i1},v_{i2},v_{i3},v_{i4})$ from T-mesh topology using a ray-tossing method introduced in [28].

Figure 3(a) shows a T-mesh with 57 junctions which includes 12 T-junctions. Bicubic B-spline functions are anchored at these junctions, and B_8 in Figure 3(a) is a bicubic B-spline function located at T-junction T_8. By applying the ray-tossing method at T_8 in four directions, B_8 gets its local-support of $(u_5,u_6,u_8,u_9,u_{10})/(v_3,v_4,v_5,v_6,v_7)$ that are two sets of knot vectors. After all the B-spline functions determine their local-supports from T-mesh topology, we can use the Equation (3.1) to construct a T-splines as shown in Figure 3(b), by assigning a specific control polygon formed by a set of control points P_i.

$$S(u,v)=\sum_{i=1}^{n}B_i(u,v)\times P_i \tag{3.1}$$

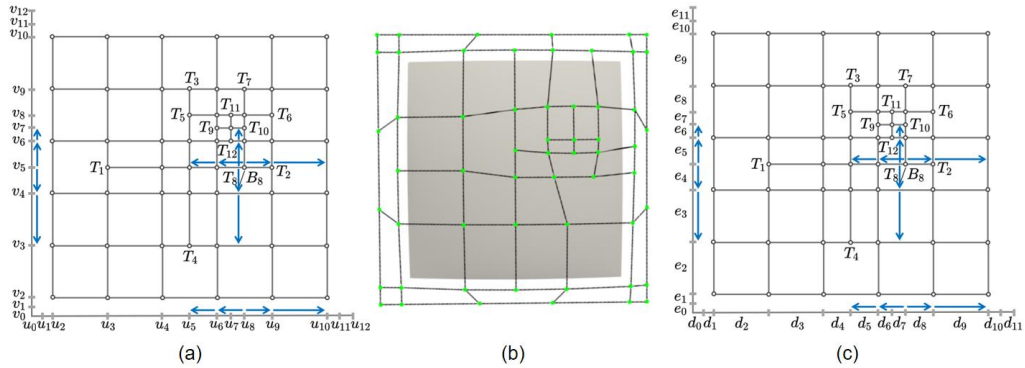

Figure 3: T-mesh can be defined over two global knot vectors (a) or two global knot intervals (c). (b) is the corresponding T-splines assigned with a control polygon.

By applying the $d_i=u_{i+1}-u_i$ and $e_i=v_{i+1}-v_i$, we can also use the knot intervals to describe the local support of each B-spline function over T-mesh. As seen in Figure 3(c), local-support of B_8 at T_8 can be redefined through knot intervals of (d_5,d_6+d_7,d_8,d_9) $/(e_3,e_4,e_5,e_6)$. Next, we will use the knot intervals to investigate an important property of LU-Refinement, which was first proposed in [28] and is one of the common refining operations for T-splines.

Figure 4 shows a typical LU-Refinement of bicubic T-splines when the new junction J' is added onto a horizontal edge of T-mesh. At this point, four neighboring B-spline functions of $B_a/B_b/B_c/B_d$ are affected by the added J' and they have uniform vertical local supports. The $d_l/d_m/d_n/d_p/d_q$ are a set of knot intervals that are used in local refinements of $B_a/B_b/B_c/B_d$. After the LU-Refinement, $B_a/B_b/B_c/B_d$ convert to the $B_a^{'}/B_b^{'}/B_c^{'}/B_d^{'}/B_e^{'}$, adding a new junction onto T-mesh and splitting the knot interval d_n into $d_n^L+d_n^R$.

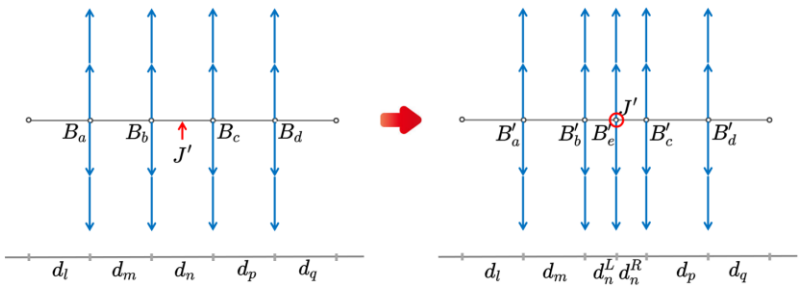

Figure 4: Local-uniform refining operation of T-splines.

According to the refinement equations of the bicubic B-spline function in four different cases that are given in Section 4.1 of [27], we use the knot intervals of $d_l / d_m / d_n^L / d_n^R / d_p / d_q$ to describe local refinements of $B_a / B_b / B_c / B_d$ in LU-Refinement and obtain the Equations (3.2) to (3.5).

$$B_a = B_a^{'} + \frac{d_n^R}{d_L + d_m + d_n} B_b^{'} \tag{3.2}$$

$$B_b = \frac{d_L + d_m + d_n^L}{d_L + d_m + d_n} B_b^{'} + \frac{d_n^R + d_p}{d_m + d_n + d_p} B_e^{'} \tag{3.3}$$

$$B_c = \frac{d_m + d_n^L}{d_m + d_n + d_p} B_e^{'} + \frac{d_n^R + d_p + d_q}{d_n + d_p + d_q} B_c^{'} \tag{3.4}$$

$$B_d = \frac{d_n^L}{d_n + d_p + d_q} B_c^{'} + B_d^{'} \tag{3.5}$$

By adding up the both sides of Equations (3.2) to (3.5), we can get the Equation (3.6).

$$B_a + B_b + B_c + B_d = B_a^{'} + B_b^{'} + B_c^{'} + B_d^{'} + B_e^{'} \tag{3.6}$$

[28] introduced the standard T-splines, whose B-spline functions meet the requirement of $\sum_{i=1}^{n} B_i(u,v) = 1$. If LU-Refinement is applied to one standard T-splines with n B-spline functions, we can always obtain another new standard T-splines, based on the deduction in Figure 5 and Equation (3.6).

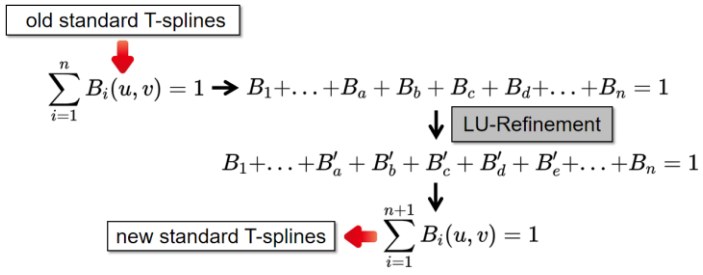

Figure 5: Pass down the standard property of T-splines through LU-Refinement.

Such a relationship between LU-Refinement and standard T-splines is quite useful in studying the analysis-suitability of MT-splines, which will be discussed in the next section.

4 MECHANICAL T-SPLINES

Compared with other types of engineering structures, the thin-shell structure has the advantages of lightness, high strength, and good design ability. Hence, thin-shell structures are extensively used to design industrial and consumer products in many applications. Due to the thin and curved characteristics of shape, a thin-walled structure in engineering is normally described through a freeform surface model in CAD, like the Bezier surface, B-spline surface, or NURBS surface. In this paper, we choose the flexible T-splines to describe the CAD model of the thin-walled product that has a freeform shape.

4.1 Isogeometric Shell Analysis

The thin-shell mechanical analysis based on isogeometric analysis has been described with details in [21]. In Kirchhoff-Love shell theory, the following two hypothesis need to be maintained.

(a) Cross-sections of the shell remain straight and perpendicular to the mid-surface during shell deformation.

(b) There are no transverse shear strains when deforming the shell structure, such as the car-body part.

The geometry of a thin-shell structure with uniform thickness can be thus represented by its mid-surface and thickness, and a linear strain distribution is ensured through the thickness.

Consider a shell model with a thickness t in the reference configuration, the mid-surface Ω is parameterized by the coordinates θ_1 and θ_2. Any material point $\overline{P}$ in the shell can be mathematically described as:

$$\overline{P}(\theta_1,\theta_2,\theta_3) = x(\theta_1,\theta_2) + \theta_3 a_3(\theta_1,\theta_2), \qquad \theta_3 \in [-\frac{t}{2},\frac{t}{2}] \tag{4.1}$$

$x(\theta_1,\theta_2)$ is the parametric representation of the middle surface of the shell. $a_3(\theta_1,\theta_2)$ is the normal vector of the point at $x(\theta_1,\theta_2)$, and can be defined as follows:

$$a_\alpha = x_{,\alpha} \qquad \alpha \in \{1,2\} \qquad a_3 = \frac{a_1 \times a_2}{|a_1 \times a_2|} \tag{4.2}$$

Where $x_{,\alpha}$ denotes the partial derivatives of x. a_1 and a_2 respectively correspond to two tangent vectors of mid-surface at $\overline{P}$.

Similarly, any material point $\hat{P}$ in the deformed geometry can be written as:

$$\hat{P}(\theta_1,\theta_2,\theta_3) = \hat{x}(\theta_1,\theta_2) + \theta_3 \hat{a}_3(\theta_1,\theta_2), \qquad \theta_3 \in [-\frac{t}{2},\frac{t}{2}] \tag{4.3}$$

Where $\hat{x}$ and $\hat{a}_3$ are defined in the same way as the x and a_3 in Equation (4.1).

Accordingly, we can obtain the displacement field $u(\theta_1,\theta_2)$ of the middle surface of the shell as follows:

$$u(\theta_1,\theta_2) = \hat{x}(\theta_1,\theta_2) - \bar{x}(\theta_1,\theta_2) \tag{4.4}$$

Such a displacement field u is enough to fully describe the kinematics of a deformed shell model under external force. All strain quantities of interest for mechanics analysis can be deduced from this displacement field u, which describes the deformation of the shell's middle surface.

For the sake of brevity, the full derivation of the thin-shell energy and equilibrium configuration, as well as the discretization of the thin-shell element, can be found in [8]. We closely follow the approaches in [8] and [25] to implement the isogeometric analysis of thin-shell based on Kirchhoff-Love theory and extend them to the case of bicubic T-splines in this paper.

4.2 Construction of MT-splines

Next, we apply the isogeometric shell analysis based on Kirchhoff-Love theory to build the MT-splines, which seamlessly combines the T-splines geometric model with the thin-shell isogeometric analysis model.

As seen in Equation (3.1) and Equation (4.5), the B-spline function $B_i(u,v)$ is not only used to define the geometry model of MT-splines in CAD by pairing with the control point P_i in $S(u,v)$, but also applied to formulate the displacement field $D(u,v)$ over MT-splines in CAE analysis by associating with the displacement variable X_i at P_i. A workflow for isogeometric shell analysis on MT-splines is shown in Figure 6, and $[K][X]=[F]$ is the resulting global stiffness matrix equation, which is the core part of MT-splines to realize shape modification and mechanical analysis.

$$D(u,v)=\sum_{i=1}^{n} B_i(u,v)\times X_i \tag{4.5}$$

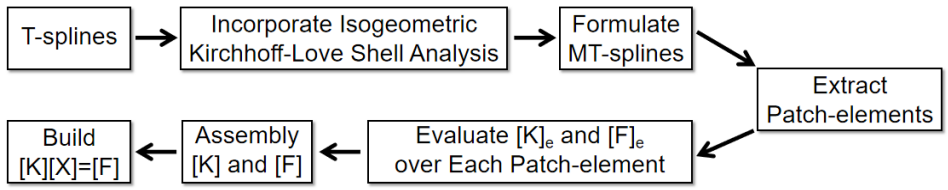

Figure 6: Isogeometric analysis workflow on MT-splines starting from T-splines.

It is desirable to have a MT-splines that is always suitable for IGA. In this paper, we will achieve this goal by utilizing the standard property and LU-Refinement of T-splines.

First of all, the Lemma 2 proposed in Section 2 of [32] has proven that standard T-splines always have a set of linearly independent B-spline functions. Hence, standard T-splines are inherently suitable for IGA. From the discussion in Section 3 about the relationship between standard T-splines and LU-Refinement, we can always generate a new standard T-splines TS_{i+1} after applying the LU-Refinement to one standard T-splines TS_i. Since TS_i and TS_{i+1} are both standard, they are linearly independent from the Lemma 2 in [32] and are suitable to IGA .

Therefore, if we start with initial MT-splines with standard property and apply LU-Refinements to refine these MT-splines for m times, we can get the $\mathrm{MTS}_1 \rightarrow \mathrm{MTS}_2 \rightarrow \ldots \rightarrow \mathrm{MTS}_m$. From above discussion, all of these MT-splines are standard and so they are also analysis-suitable T-splines. In Figure 7, for example, TS_0 is a standard T-spline and is converted to a MT-splines MTS_0 after incorporating isogeometric shell analysis. MTS_0 inherits the standard property from TS_0.

Next, we apply LU-Refinements to refine MTS_0 to the MTS_1 by adding a local row of control points. Then, we continue to refine MTS_1 to the MTS_2 through LU-Refinements and add another local column of control points. Because MTS_1 and MTS_2 are produced from the initial standard MTS_0 by applying only LU-Refinements, they are both standard like MTS_0, and $\mathrm{MTS}_0 / \mathrm{MTS}_1 / \mathrm{MTS}_2$ are all suitable for IGA.

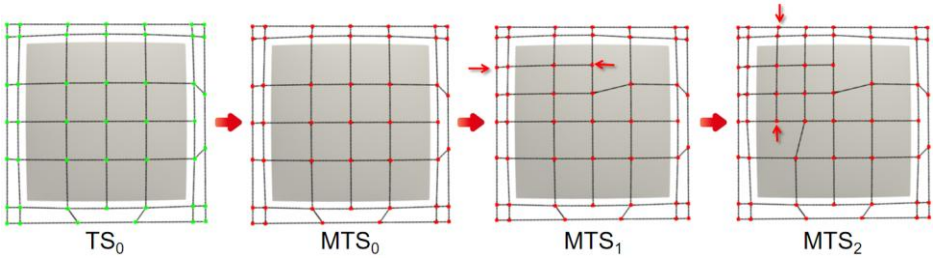

Figure 7: An example of how to ensure the analysis-suitability of MT-splines during local refinements.

In this way, we can always guarantee the analysis-suitability of MT-splines for IGA during local refinements, which will help us to realize the intuitive deformation design and direct mechanical analysis of MT-splines driven by isogeometric shell analysis.

5 INTEGRATED PRODUCT REDESIGN WORKFLOW

To streamline the redesign process of the thin-walled product whose CAD documents are not complete enough to reconstruct the CAD model of this product, we propose a new redesign workflow for the thin-walled product, as seen in Figure 8, by combining the reverse modeling technique, LU-Refinements of T-splines and isogeometric analysis of thin-shell.

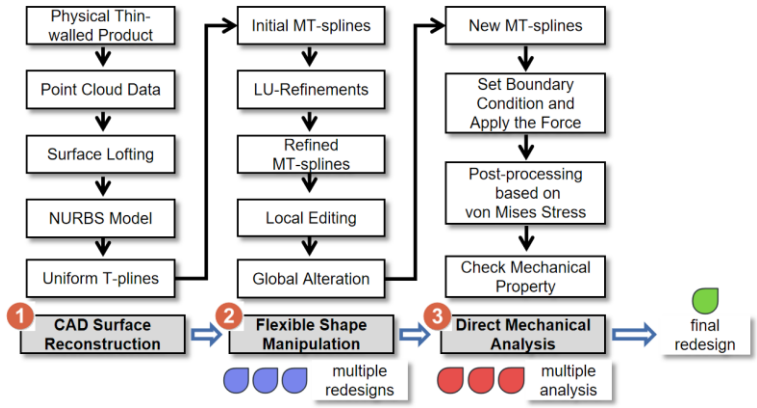

Figure 8: New workflow for thin-walled product redesign based on three major steps.

Step 1：CAD Surface Reconstruction.

Firstly, we use a 3D optical scanner to acquire the shape information about physical thin-walled product. A point-cloud data is produced and processed into a suitable mesh model for surface

reconstruction. Then, we create multiple spline curves over the mesh model and reconstruct a NURBS model through surface lofting. Finally, the reconstructed NURBS model is exactly converted to uniform T-splines without T-junctions by redefining B-spline functions from the tensor-product spline scheme to the PB-splines scheme based on T-mesh. This step offers a proper CAD model described by uniform T-splines for subsequent product redesign and is the foundation of workflow.

Step 2：Flexible Shape Manipulation.

In this step, uniform T-splines are incorporated with isogeometric shell analysis to build an initial MT-splines. Because uniform T-splines have the same set of B-spline functions as the NURBS model after exact conversion between them, initial MT-splines also possess the standard property of $\sum B_i = 1$. Then, local rows or columns of new control points are added over MT pipelines through LU-Refinements. From the discussion in Section 4, LU-Refined MT-splines are also standard and are thus suitable for IGA all the time.

We can efficiently create new local details by editing those locally added control points through geometric displacements. After editing local details over MT-splines, we can realize the global alteration of MT-splines via mechanical deformation based on $[X]=[K]^{-1}[F]$, which is derived from the $[K][X]=[F]$ in isogeometric shell analysis. By applying a force vector of $[F_{\mathrm{CAD}}]$ onto MT-splines for shape design, we can obtain a global displacement vector of $[X_{\mathrm{CAD}}]=[K]^{-1}[F_{\mathrm{CAD}}]$. Each X_i in $[X_{\mathrm{CAD}}]$ is a displacement value to be used to update the position of the control point P_i to achieve the global alteration of MT-splines.

In this way, we can realize the flexible shape manipulation of MT-splines through local geometric editing as well as global mechanical alteration, producing multiple redesign schemes for thin-walled products. This step is the core part of the entire redesign workflow.

Step 3：Direct Mechanical Analysis

Surface patches of MT-splines serve as finite elements in isogeometric shell analysis in this step. Hence, we can directly conduct the mechanical analysis over MT-splines based on $[K][X]=[F]$ that results from isogeometric shell analysis by skipping the complex and time-consuming finite element meshing. Specifically, we get the $[X_{\mathrm{CAE}}]=[K]^{-1}[F_{\mathrm{CAE}}]$ by applying a force vector $[F_{\mathrm{CAE}}]$ onto MT-splines for mechanical analysis. X_i is the displacement value in $[X_{\mathrm{CAE}}]$ and is put back into the $D(u,v)=\sum_{i=1}^{n} B_i(u,v)\times X_i$, which is post-processed to generate a stress distribution on MT-splines to describe the effect of $[F_{\mathrm{CAE}}]$. By doing this, we can greatly simplify the analysis process in CAE and quickly check the mechanical property of redesigned thin-walled product.

A decision on the final redesign scheme will be made by comprehensively considering the mechanical analysis result and new shape of redesigned product.

Figure 9 offers an example to illustrate our proposed new workflow for thin-walled product redesign. Figures 9(a) to 9(c) describe Step 1 of CAD surface reconstruction, in which a NURBS model is reconstructed from 3D scanned data through surface lofting and is exactly converted to uniform T-splines. Figures 9(d) to 9(g) show Step 2 of flexible shape manipulation. In this step, a new local feature is firstly created over MT-splines by editing locally added control points via geometric displacements, and then the entire surface is globally altered by fixing one surface boundary and applying an upper force. Figure 9(h) represents Step 3 of direct mechanical analysis over MT-splines without needing the additional finite element meshing process. Next, we will determine whether the MT-splines resulting from flexible shape manipulation can be used as the final redesign scheme, based on the analysis result in Figure 9(h) and the new shape in Figure 9(g).

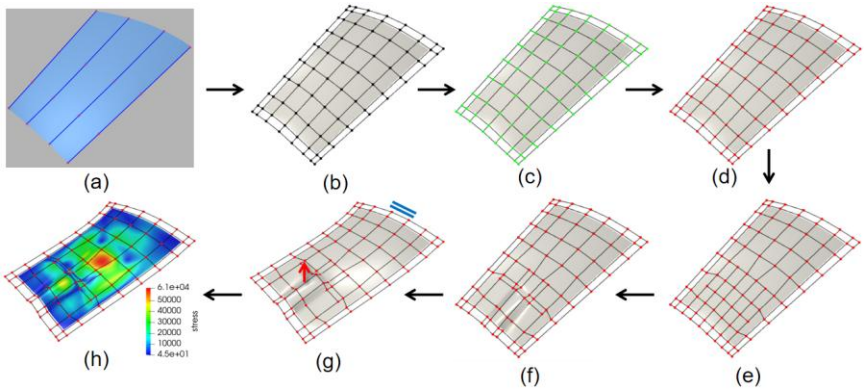

Figure 9: Application of our proposed new workflow for thin-walled product redesign: (a) Scanned data with added lofting curves, (b) Recreated NURBS model, (c) Exactly converted uniform T-splines, (d) Initial MT-splines with incorporated thin-shell property, (e) LU-Refined MT-splines, (f) MT-splines after editing local details, (g) MT-splines after applying global alteration, (h) Direct analysis on the MT-splines with a new shape.

6 PRODUCT REDESIGN EXAMPLES

In this section, we will first use an example of a bike mudguard to demonstrate the usefulness and effectiveness of our proposed new workflow for thin-walled product redesign. As seen in Figure 10(a), this is one type of mudguard on the market that has become less appealing to customers in recent years for its old-fashioned style. To increase the competitiveness of this product in the market, designers are asked to develop a more sleek mudguard through product redesign. Unfortunately, the original CAD documents of this mudguard product have been lost for some reason. Hence, we will exploit the RE modeling and MT pipelines to achieve an efficient redesign of this thin-walled product.

In Figure 10(a), we place the physical mudguard product onto the turntable of the optical 3D scanner so as to obtain 3D point-cloud data about the shape of the mudguard. After completing the operations of registration, cleaning, simplification and smoothing on this point-cloud data, we acquire a mesh model for mudguard and import it into Geomagic Design X [14] for surface reconstruction. Several section curves are properly created over this mesh model by utilizing the 3D splines modeling tool in Geomagic Design X, and they are used to recreate a NURBS surface in Figure 10(b) through surface lofting to approximate the shape of the scanned mudguard.

Next, we exactly convert the NURBS surface into uniform T-splines by redefining B-spline functions over a uniform T-mesh and blend uniform T-splines with the thin-shell mechanical property through isogeometric analysis to build an initial MT-splines with 210 control points, as seen in Figure 10(c). These MT-splines will be used as a suitable CAD/CAE model for subsequent mudguard redesign.

To add some new local features onto the mudguard to increase its functionality and aesthetics, we apply LU-Refinements to locally add 80 new control points onto MT pipelines. These new control points are edited through geometric displacements to create required local features over MT-splines, obtaining the first redesign scheme of mudguards, as seen in Figure 10(d). Suppose we choose the popular NURBS modeling approach to achieve the same shape of mudguard as Figure 10(d). In that case, we have to add 310 new control points rather than 80 control points due to the global refinements of NURBS, producing a cumbersome NURBS surface in Figure 10(e) with many redundant control points.

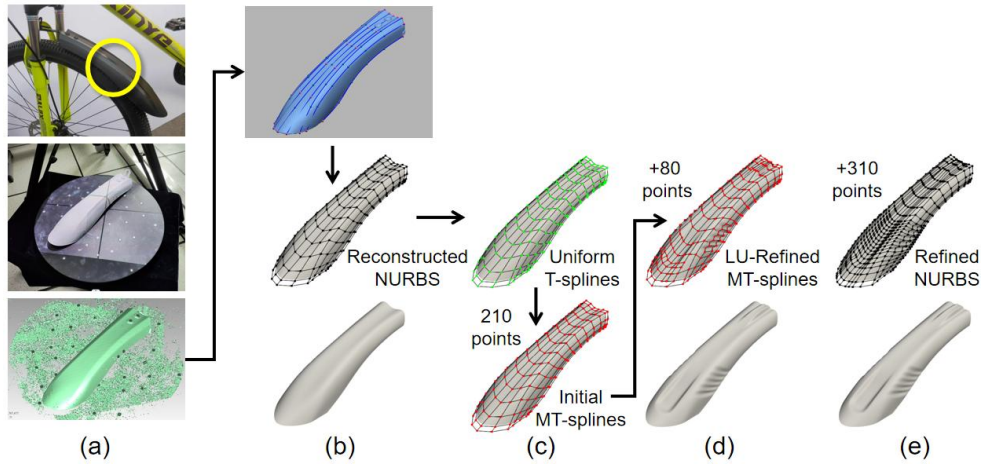

Figure 10: Surface reconstruction and local editing of mudguard model: (a) Shape data acquisition using an optical scanner, (b) Reconstruction of NURBS surface from scanned data of mudguard through surface lofting, (c) Converted T-splines and initial MT-splines, (d) First redesign scheme for mudguard described by a compact MT-splines that results from LU-Refinements and local editing, (e) Same modeling result achieved by using a refined NURBS surface with many unnecessary control points.

Here, we can see that MT-splines is capable to make the local editing of mudguard in redesign process more flexible and efficient through local refinements than common NURBS surface. Moreover, a compact MT-splines geometry can be produced with the advantage of facilitating subsequent redesign operations on the mudguards, including the deformation alteration and mechanical analysis.

Particularly, we only apply LU-Refinements to refine MT-splines throughout the local editing of the mudguard. Hence, the LU-Refined MT-splines in Figure 10(d) have the standard property to be linearly independent and are suitable for IGA, based on the discussion in Section 4. In this way, we can reliably employ isogeometric shell analysis to realize the intuitive deformation alteration and direct mechanical analysis of mudguards in CAD and CAE, respectively.

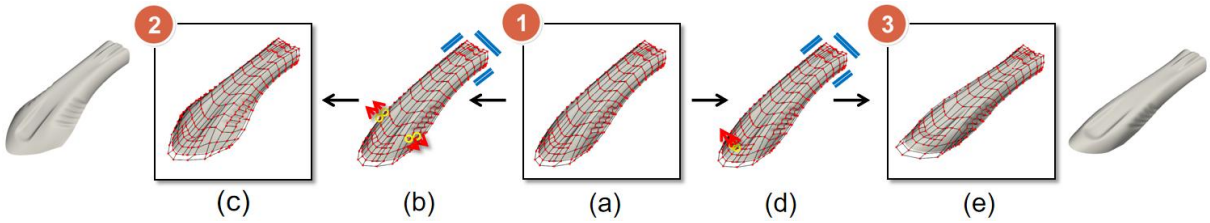

Figure 11: Global deformation alteration of mudguard driven by isogeometric shell analysis: (a) First redesign scheme for the mudguard, (b)(c) Deform the mudguard to get the second redesign, (d)(e) Deform the mudguard to obtain the third redesign.

Based on the first redesign of the mudguard in Figure 11(a) that results from local editing, we can easily obtain another two redesigns for the mudguard by utilizing the mechanical deformation of MT-splines driven by isogeometric shell analysis. As seen in Figure 11(b), we fix the upper end of MT-splines and apply two outward forces onto two points on both sides of the mudguard. $[X_{\mathrm{CAD}}]$ is

computed from the stiffness matrix equation of $[X_{\text{CAD}}]=[K]^{-1}[F_{\text{CAD}}]$ inside MT-splines and is used to deform the shape of MT-splines by updating control points, generating the second redesign of mudguard in Figure 11(c). As shown in Figure 11(d), we similarly keep the upper end of MT-splines fixed and exert two upper forces onto another two points over MT-splines this time. According to the computed $[X_{\text{CAD}}]$, mudguard is smoothly deformed to produce the third redesign in Figure 11(e).

Comparing with the redundant NURBS surface in Figure 10(e), the compact geometry of MT-splines shown in Figure 10(d) is more advantageous to realize the efficient deformation alteration of mudguard in Figure 11 controlled by isogeometric shell analysis .

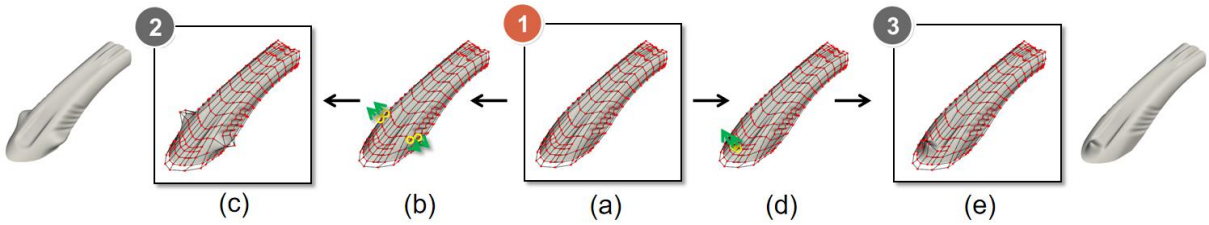

Figure 12: Undesirable modification of mudguard produced from traditional geometry editing: (a) First redesign scheme for the mudguard, (b)(c) Local editing effect different from the second redesign scheme, (d)(e) Local editing effect, unlike the third redesign scheme.

If we choose to edit the shape of mudguard by displacing these control points in a common geometric way rather than in a manner of mechanical deformation as described above, we can only get the undesirable results of local modification as seen in Figure 12. Hence, the capability of mechanical deformation of MT-splines offers us more modeling flexibility for mudguard redesign than traditional geometric editing method, producing a desired smooth global modification of mudguard.

Finally, we employ the direct mechanical analysis of MT-splines to efficiently check the mechanical property of each redesigned mudguard, so as to choose a best redesign scheme.

In Figure 13(a), we set identical boundary conditions and apply same downward forces over redesigned mudguards, which are all created from one existing physical mudguard product by applying the reverse modeling, local geometric editing and global deformation. Mechanical analysis results for these mudguards can be quickly obtained in Figure 13(b), after post-processing the computed displacement vector of $[X_{\text{CAE}}]=[K]^{-1}[F_{\text{CAE}}]$ based on von Mises stress distribution. Here, the material properties are the Poisson's ratio ν =0.25 and Young's modulus E=1.6x10^{6}N/mm^2, and the thickness t=2mm.

By making full use of the seamless integration between CAD and CAE within MT-splines, we can easily bypass the complicated process of finite element meshing as required in common CAE analysis, which can be seen from Figures 13(a) to 13(c). As a result, the efficiency of mechanical analysis in the final step of mudguard redesign workflow is significantly improved.

Moreover, the compact set of B-spline functions in MT-splines after LU-Refinements makes it more efficient to achieve the isogeometric shell analysis on mudguard than the case of using a redundant NURBS model produced from full rows and columns of refinements.

After comparing three mechanical analysis results shown in Figure 13(b), we select the third redesign scheme as the final candidate to develop the coming new mudguard product, because this scheme has a better mechanical property without the concentration of stresses than the other two schemes. This redesign scheme for mudguard achieves a good trade-off between aesthetic appearance and mechanical performance.

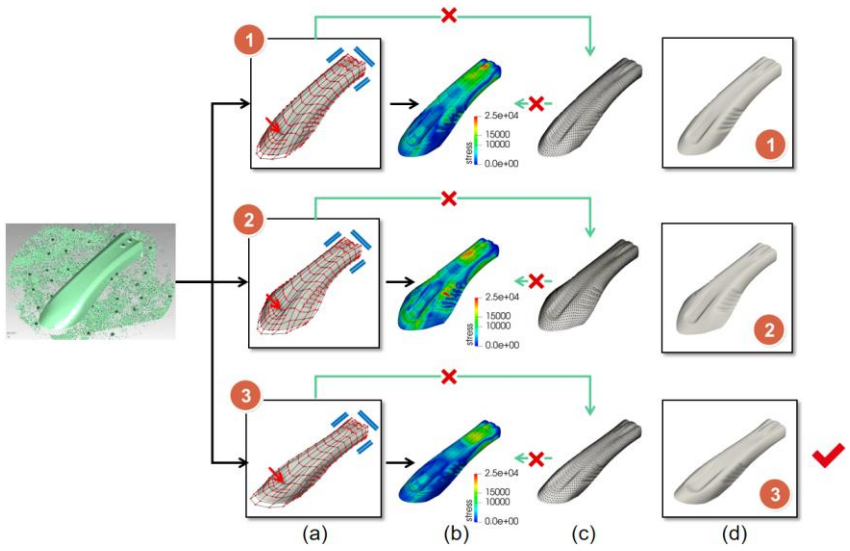

Figure 13: Verification of redesign schemes through the direct mechanical analysis of MT-splines: (a) Impose same boundary conditions and forces on redesigned mudguard models before the analysis, (b) Isogeometric analysis results, (c) Conventional finite element models of mudguards necessary for CAE analysis, (d) Alternative schemes of redesigned mudguard for comparison.

To further demonstrate the benefit and usefulness of our proposed new method, we offer another example in automotive styling about the redesign of car-door. However, our existing optical 3D scanner shown in Figure 10(a) is limited to acquiring the surface data of small parts like the mudguard, not the components as large as the car door. Hence, we download an existing point-cloud data set of bodywork from [15], whose scanned data about the car door is utilized in this redesign example.

The whole redesign process of the car door is similar to the case of the mudguard as described above. As seen in Figure 14(a) and Figure 14(b), we reconstruct a NURBS model from the scanned data of the car door through surface lofting and take it as the original design for the car door. In Figure 14(c) and Figure 14(d), the reconstructed NURBS model is firstly converted to uniform T-splines and then initial MT-splines, which are refined through LU-Refinements and edited by adding desired local features. The LU-Refined MT-splines in Figure 14(d) use a more compact geometry than the refined NURBS in Figure 14(e) to achieve the same car-door surface design.

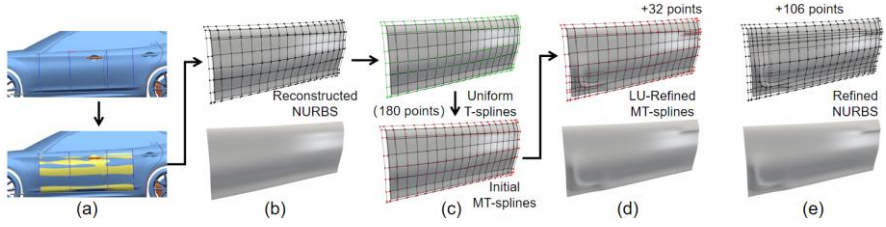

Figure 14: Surface reconstruction and local editing of car-door model: (a) Surface lofting applied on a scanned point-cloud data of car-door, (b) NURBS surface after reconstruction, (c) Conversion into a T-splines and an initial MT-splines, (d) First redesign scheme for car-door represented by a compact MT-splines after LU-Refinements and local editing, (e) Same modeling result produced from a refined NURBS surface with many redundant control points.

After we obtain the first redesign scheme for the car-door in Figure 15(a) by editing locally added control points, we apply the isogeometric shell analysis model within MT-splines to realize the mechanical deformation of car-door geometry, producing the second and third redesign schemes as shown in Figures 15(b) to 15(e). These two new schemes for the car door in Figure 15, resulting from the mechanical deformation, have much smoother appearances than the other two car-door redesign schemes in Figure 16, which are generated by moving the same set of control points in a traditional geometric manner. In the redesign process of car door here, the material properties used in isogeometric shell analysis are the Poisson's ratio ν =0.25 and Young's modulus E=1.6x10^{6}N/mm^2, and the thickness t=1.5mm.

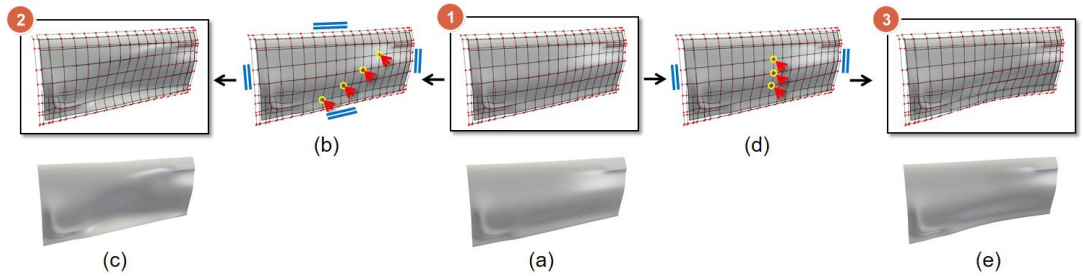

Figure 15: Smooth global deformation of car-door controlled by isogeometric shell analysis: (a) First redesign scheme of car-door, (b)(c) Deform the car-door to produce the second redesign by fixing four boundaries and applying forces onto four control points inwards, (d)(e) Deform the car-door to obtain the third redesign after fixing the left and right boundaries and applying forces to three control points inwards.

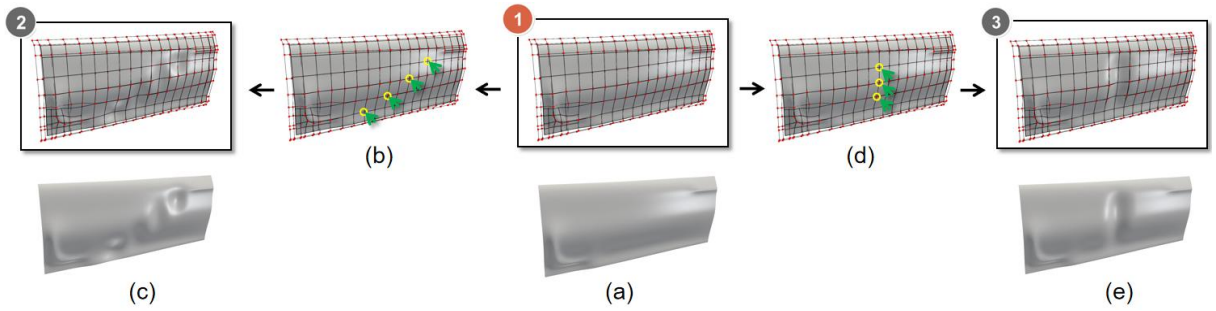

Figure 16: Unwanted shape alteration of car-door resulting from traditional geometry editing: (a) First redesign scheme of car-door, (b)(c) Local editing result corresponding to the second redesign by moving four control points inwards, (d)(e) Local editing result corresponding to the third redesign after moving three control points inwards.

In Figure 17, we employ the efficient direct mechanical analysis of MT-splines to verify the mechanical properties of three redesigned car-doors without the need to convert them into complex finite element models in Figure 17(c). By comparing the analysis results in Figure 17(b), the second redesign scheme is discarded for its acute stress concentration, and the other two schemes have similar good mechanical performances. Next, we further compare the first scheme with the third scheme and finally decide to choose the third one as the final candidate for the style design of the new car door. It is because the third redesign scheme offers a more sleek and fashionable appearance than the first scheme to enhance the aesthetic appeal for customers, as seen in Figure 17(d).

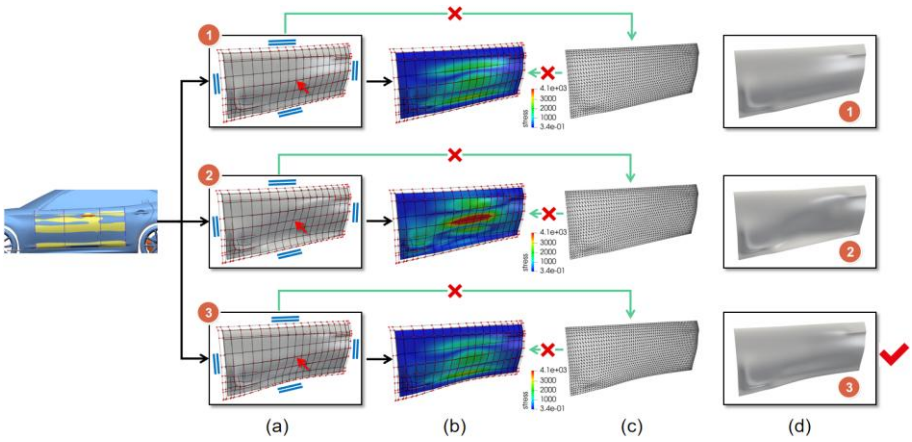

Figure 17: Verification of redesign schemes based on the direct mechanical analysis of MT-splines: (a) Impose same boundary conditions and forces on redesigned car-door models before the analysis, (b) Isogeometric analysis results, (c) Conventional finite element models of car-doors required for CAE analysis, (d) Different appearances of redesigned car-door used for comparison.

7 CONCLUSION AND DISCUSSION

In this paper, we propose a new approach to streamline the redesign workflow of thin-walled product, based on the CAD surface reconstruction, flexible shape manipulation and direct mechanical analysis. Firstly, RE modeling is used to obtain a suitable NURBS model from one physical thin-walled product, whose original CAD data is either incomplete or unavailable. Then, we convert this NURBS model into a MT-splines through isogeometric shell analysis, so that we can achieve the flexible shape manipulation of thin-walled product via local geometric editing as well as global mechanical deformation. Next, we employ the direct mechanical analysis of MT-splines to rapidly check the mechanical properties of multiple redesigned thin-walled products, so as to choose the most desirable one. In the end, redesign examples of mudguard and car-door are given to show the effectiveness and usefulness of our proposed new redesign workflow for thin-walled product.

During the redesign process of thin-walled product described by MT-splines, we particularly adopt the LU-Refinement to refine MT-splines to ensure the standard property of MT-splines all the time. As a result, LU-Refined MT-splines can be always linearly-independent and suitable for IGA, effectively tackling the tricky issue of analysis-suitability for MT-splines after local refinements. In this way, we can enable the global mechanical deformation and direct mechanical analysis of MT-splines to be reliably driven by isogeometric shell analysis, greatly improving the redesign workflow of thin-walled product in both aspects of CAD and CAE. Moreover, MT-splines can produce a more compact CAD geometry than the popular NURBS surface after refinements, making the shape manipulation and mechanical analysis in thin-walled product redesign more efficient.

The MT-splines introduced in this paper is limited to the redesign of thin-walled product, which is defined over a single rectangular domain. To make our proposed new redesign approach more useful in practical application, we will extend MT-splines to the complex multi-rectangular domain with more than four boundaries in our following study. The analysis-suitable unstructured T-splines developed in [33] will be one of our research focuses to achieve this goal. Additionally, we will explore to integrate the digital photogrammetry technology [20], which is widely used in the 3D digital reconstruction of heritage artifacts, into the process of reverse modeling. By doing this, we hope to develop a more cost-effective workflow for thin-walled product redesign by giving up the use of expensive 3D scanners in CAD surface reconstruction.

Xiang Xue, https://orcid.org/0000-0001-6125-3122

Xiaolian Tang, https://orcid.org/0009-0004-0608-5962
Xiaoyun Qiu, https://orcid.org/0009-0006-7731-1132

REFERENCES

[1] Abaqus, https://www.3ds.com/products/simulia/abaqus , SIMULIA, Dassault Systèmes.
[2] Aung, T.L.; Ma, N.; Kishida, K.; Guzik, A.: Advanced structural health monitoring method by integrated isogeometric analysis and distributed fiber optic sensing, Sensors, 2021, 21(17), 5794. https://doi.org/10.3390/s21175794
[3] Bazilevs, Y.; Takizawa, K.; Tezduyar, T.E.; Korobenko, A.; Kuraishi T.; Otoguro, Y.: Computational aerodynamics with isogeometric analysis, Journal of Mechanics, 2023, 39, 24-39. https://doi.org/10.1093/jom/ufad002
[4] Bucelli, M.; Salvador, M.; Dede', L.; Quarteroni, A.: Multipatch isogeometric analysis for electrophysiology: Simulation in a human heart, Computer Methods in Applied Mechanics and Engineering, 2021, 376, 113666. https://doi.org/10.1016/j.cma.2021.113666
[5] Buonamici, F.; Carfagni, M.; Furferi, R.; Governi, L.; Lapini, A.; Volpe, Y.: Reverse engineering modeling methods and tools: A survey, Computer-Aided Design and Applications, 2018, 15(3), 443 – 464. https://doi.org/10.1080/16864360.2017.1397894
[6] CATIA, https://www.3ds.com/products-services/catia/disciplines/designstyling/, Dassault Systèmes.
[7] Cheng, S.-Y.; Yang, X.-R; Zhang, X.-W.; Liang, S.-Q.: A redesign methodology for Reverse Engineering integrated with haptic modeling, 2010 The 2nd International Conference on Computer and Automation Engineering (ICCAE), Singapore, 2010, 105-108. https://doi.org/10.1109/ICCAE.2010.5452050
[8] Cirak, F.; Ortiz, M.; Schröder, P.: Subdivision surfaces: a new paradigm for thin-shell finite-element analysis, International Journal for Numerical Methods in Engineering, 47(12), 2039-2072. https://onlinelibrary.wiley.com/doi/10.1002/(SICI)1097-0207(20000430)47:12%3C2039:: AID-NME872%3E3.0.CO;2-1
[9] Cottrell, J.A.; Reali A.; Bazilevs, Y.; Hughes T.J.R.: Isogeometric analysis of structural vibrations, Computer Methods in Applied Mechanics and Engineering, 2006, 195(41-43), 5257-5296. https://doi.org/10.1016/j.cma.2005.09.027
[10] Dimitri, R.; Lorenzis, L.D.; Scott, M.A.; Wriggers, P.; Taylor, R.L.; Zavarise, G.: Isogeometric large deformation frictionless contact using T-splines, Computer Methods in Applied Mechanics and Engineering, 2014, 269, 394-414. https://doi.org/10.1016/j.cma.2013.11.002
[11] Dörfel M.R.; Jüttler, B.; Simeon, B.: Adaptive isogeometric analysis by local h-refinement with T-splines, Computer Methods in Applied Mechanics and Engineering, 2010, 199(5-8), 264-275. https://doi.org/10.1016/j.cma.2008.07.012
[12] Feng, J.-W.; Fu, J.-Z.; Lin, Z.-W.; Shang C.; Li B.: Direct slicing of T-spline surfaces for additive manufacturing, Rapid Prototyping Journal, 2018, 24(4), 709-721. https://doi.org/10.1108/RPJ-12-2016-0210
[13] Gan, W.-F.; Fu, J.-Z.; Shen, H.-Y.; Chen, Z.-Y.; Lin Z.-W.: Five-axis tool path generation in CNC machining of T-spline surfaces, Computer-Aided Design, 2014, 52, 51-63. https://doi.org/10.1016/j.cad.2014.02.013
[14] Geomagic Design X, https://oqton.com/geomagic-designx/, Oqton.
[15] GrabCAD Community, https://grabcad.com/library, GrabCAD.
[16] Greco, F.; Coox, L.; Maurin, F.; Balla, V.K.; Deckers, E.; Desmet, W.: Reverse engineering of deep drawn components with an isogeometric framework, Computers & Structures, 2018, 201, 15-25. https://doi.org/10.1016/j.compstruc.2018.02.010
[17] Hartmann, S.; Benson, D.J.; Nagy, A.P.: Isogeometric analysis with LS-DYNA, Journal of Physics: Conference Series, 2016, 734. https://doi.org/10.1088/1742-6596/734/3/032125
[18] Hughes, T.J.R.; Cottrell J.A.; Bazilevs Y.: Isogeometric analysis: CAD, finite elements, NURBS, exact geometry and mesh refinement, Computer Methods in Applied Mechanics and Engineering, 2005, 194(39-41), 4135-4195. https://doi.org/10.1016/j.cma.2004.10.008

[19] Joshi, K.; Bhatt, A.D.: Development of multi-branch T-spline templates and its applications in reverse engineering, Computer-Aided Design and Applications, 2020, 17(3), 487-501. https://doi.org/10.14733/cadaps.2020.487-501
[20] Kaufman, J.; Rennie, A.E.; Clement, M.: Single camera photogrammetry for reverse engineering and fabrication of ancient and modern artifacts, Procedia CIRP, Volume 36, 2015, 223-229. https://doi.org/10.1016/j.procir.2015.01.073
[21] Kiendl J.; Bletzinger K.-U.; Linhard J.; Wüchner R.: Isogeometric shell analysis with Kirchhoff-Love elements, Computer Methods in Applied Mechanics and Engineering, 2009, 198(49-52), 3902-3914. https://doi.org/10.1016/j.cma.2009.08.013
[22] Lai, Y.-C.; Zhang, Y.-J.; Liu, L.; Wei, X.-D.; Fang, E.; Lua, J.: Integrating CAD with Abaqus: A practical isogeometric analysis software platform for industrial applications, Computers & Mathematics with Applications, 2017, 74(7), 1648-1660. https://doi.org/10.1016/j.camwa.2017.03.032
[23] Lorenzis, L.D.; Wriggers P.; Hughes, T.J.R.: Isogeometric contact: a review, GAMM-Mitteilungen, 2014, 37(1), 85-123. https://doi.org/10.1002/gamm.201410005
[24] Nasri, A.; Sinno, K; Zheng, J.-M.: Local T-spline surface skinning, The Visual Computer, 28, 2012, 787 – 797. https://doi.org/10.1007/s00371-012-0692-1
[25] Nguyen, V.P.; Anitescu, C.; Bordas, S.P.A.; Rabczuk, T.: Isogeometric analysis: An overview and computer implementation aspects, Mathematics and Computers in Simulation, 117, 2015, 89-116. https://doi.org/10.1016/j.matcom.2015.05.008
[26] NX CAD, https://plm.sw.siemens.com/en-US/nx/cad-online/mcad-software/industrial-product-design/, Siemens Digital Industries Software.
[27] Sederberg, T.W.; Cardon, D.L.; Finnigan, G.T.; North, N.S.; Zheng, J.M.; Lyche, T.: T-spline simplification and local refinement, ACM Transactions on Graphics, 23(3), 2004, 276-283. https://doi.org/10.1145/1015706.1015715
[28] Sederberg, T.W.; Zheng, J.M.; Bakenov, A.; Nasri A.: T-splines and T-NURCCs, ACM SIGGRAPH 2003, 2003, 477-484. https://doi.org/10.1145/1201775.882295
[29] Smith S.; Smith G.; Shen Y.-T.: Redesign for product innovation, Design Studies, 33(2), 2012, 160-184. https://doi.org/10.1016/j.destud.2011.08.003
[30] Teschemacher, T.; Bauer, A.M.; Oberbichler, T.; Breitenberger M.; Rossi R.; Wüchner R.; Bletzinger K.-U.: Realization of CAD-integrated shell simulation based on isogeometric B-Rep analysis, Advanced Modeling and Simulation in Engineering Sciences, 2018, 5, 19. https://doi.org/10.1186/s40323-018-0109-4
[31] ThinkDesign CAD, https://www.dptcorporate.com/, DPTLab.
[32] Wang, A.-Z.; Zhao, G.: An algorithm of determining T-spline classification, Expert Systems with Applications, 2013, 40(18), 7280-7284. https://doi.org/10.1016/j.eswa.2013.07.029
[33] Wei, X.-D.; Li X.; Qian, K.-R.; Hughes, T.J.R.; Zhang, Y.-J.; Casquero, H.: Analysis-suitable unstructured T-splines: Multiple extraordinary points per face, Computer Methods in Applied Mechanics and Engineering, 2022, 391, 114494. https://doi.org/10.1016/j.cma.2021.114494
[34] Yang, J.-H.; Cheng, S.-Y.; Yang, X.-R.; Zhang, X.-W.; Luo, S.-M.: Parametric reverse modeling and redesign method of prismatic shapes, In: Jin, D., Lin, S. (eds) Advances in Future Computer and Control Systems, Advances in Intelligent and Soft Computing, vol 159, Springer, Berlin, Heidelberg. https://doi.org/10.1007/978-3-642-29387-0_35
[35] Ye, X.-Z.; Liu, H.-Z.; Chen, L.; Chen, Z.-Y.; Pan, X.; Zhang, S.-Y.: Reverse innovative design — an integrated product design methodology, Computer-Aided Design, Volume 40, Issue 7, 2008, 812-827. https://doi.org/10.1016/j.cad.2007.07.006
[36] Zhao, L.-F.; Cheng, S.-Y.; Yang, X.-R.; Zhang, X.-W.: The redesign method integrated reverse modeling with deformation, In: Jin, D., Lin, S. (eds) Advances in Future Computer and Control Systems, Advances in Intelligent and Soft Computing, vol 159, Springer, Berlin, Heidelberg. https://doi.org/10.1007/978-3-642-29387-0_39